Geosciences Journal
Vol. 8, No. 4, p. 401 − 413, December 2004

Groundwater flow characterization in the vicinity of the underground caverns in fractured rock masses by numerical modeling

Hyung-Sik Yang, Jae-Gi Kang* — *Department of Geosystem Engineering, Chonnam National University, Gwangju 500-757, Korea*
Kyung-Su Kim, Chun-Su Kim — *Radioactive waste disposal research, Korea Atomic Energy Research Institute, Daejeon 305-353, Korea*

ABSTRACT: Groundwater inflow into the caverns constructed in fractured bedrock was simulated by numerical modeling: NAPSAC (DFN, discrete fracture network model) and NAMMU (CPM, continuous porous media model), which is a finite-element software package for groundwater flow in 3D fractured media developed by AEA Technology, UK. The input parameters for modeling are based on surface fracture survey, core logging and single hole hydraulic test data. In order to predict the groundwater inflow as accurately as possible, the anisotropic hydraulic conductivity was considered. The anisotropic hydraulic conductivities were calculated from the fracture network properties and the in-situ fracture data. With a minor adjustment during model calibration, the numerical modeling is able to reasonably reproduce groundwater inflows into the cavern as well as the travel lengths and the surface arrival times through the flow paths.

Key words: 3D fractured media, anisotropic hydraulic conductivitiy, DFN model, CPM model, groundwater inflows

1. INTRODUCTION

The basic principle of crude oil storage in unlined underground caverns is that the groundwater pressure of rock mass around the caverns should be higher than that of the storage cavern pressure to prevent an oil leakage toward the surrounding rock mass. Those modeling in underground caverns have been studied analytically by many researchers (Bawden, 1980; Goodall, 1986; Nakagawa et al., 1987; Watanabe et al., 1987; Goodall et al., 1988; Geostock, 1992). In the case of crystalline rock, the performance and stability of underground storage caverns depend on the fracture flows in the vicinity of the crude oil storage facilities. In particular, predicting the pathways and travel times for leaking oil is one of the most critical subjects for the performance of facilities. Also, groundwater inflows into caverns may create a potential hazard for cavern stability and are an important factor controlling the excavation rates for tunnel construction.

In this study, a fracture network based on the results of field investigations was generated. The use of a discrete fracture model for simulating a network with high fracture density is limited by computer capacity. That is particularly true when it comes to three-dimensional modeling. Thus, it may be necessary to represent the rock as an effective porous medium. For better prediction of the groundwater flow using a porous medium model, the anisotropic hydraulic conductivity of the rock should be considered. In this paper, the discrete fracture network (DFN; NAPSAC) and continuous porous media (CPM; NAMMU) concepts in three-dimensional numerical modeling were applied to analyze the groundwater flow in the vicinity of oil storage caverns. Anisotropic conductivity values for CPM numerical modeling were inversely calculated through the DFN model, which reflects the probabilistic distribution characteristic of fracture system in the study area. This paper is reported the six components of the hydraulic conductivity determine process and the result of 3D porous medium model analysis.

In order to generate a three-dimensional fracture network, CONNETFLOW was used. CONNECTFLOW (Hartley, 1996; CONtinuum and NEtwork Contaminant Transport and FLOW) is an advanced software package for modeling groundwater flow and transport in porous and fractured media. It is based on the NAMMU and NAPSAC software and provides all of the functionality of NAMMU and NAPSAC (Fig. 1). In addition, it enables combined models to be built consisting of NAMMU (porous medium) and NAPSAC (fractured rock) sub-models. The NAPSAC (Hartley et al., 1996; Hartley, 1998) is a finite-element software package for modeling groundwater flow and transport in fractured rock. A discrete fracture network approach is used to model groundwater flow and the transport of contaminants through fractured rock. The NAMMU (Hartley et al., 1998; Numerical Assessment Method for modeling Migration Underground) is a finite-element software package for modeling groundwater flow and transport in porous media. Both codes were developed by AEA Technology in UK. Those modeling packages have been widely used in many European countries and their suitability for the groundwater flow modeling around deep geological repositories has been verified (Atkinson, 1984; Robinson et al., 1986; Schwartz et al., 1991; Jenkins et al., 1995; Hartley et al., 1994; Hartley et al., 1995).

In order to build a three-dimensional fracture network,

*Corresponding author: k9406022@yahoo.co.kr

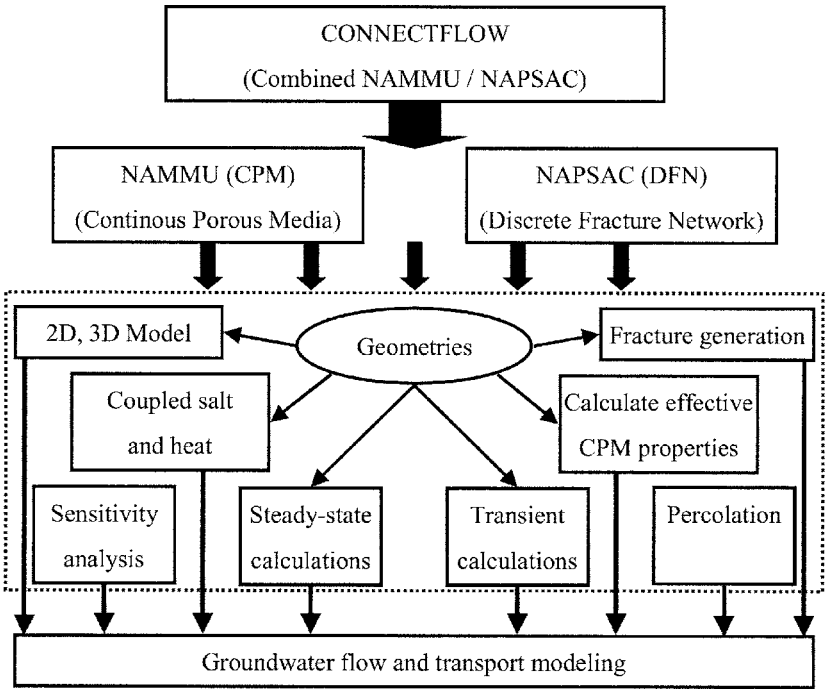

Fig. 1. NAPSAC (porous medium) and NAMMU (fractured rock) sub-model.

discontinuity data are obtained from surface fracture survey, borehole logging and BHTV (BoreHole TeleViewer) scanning images. Fracture data were analyzed to derive statistical properties for the fracture network. Important parameters that can influence the hydraulic conductivity of a rock mass include fracture orientation, aperture, fracture spacing, fracture trace length, connectivity, filling materials and fracture roughness. Among those, fracture orientation, aperture, fracture spacing, and filling material were determined from borehole logging and surface facture survey. Fracture length and connectivity, however, could not be obtained from borehole logging, but were indirectly estimated from various methods. For instance, fracture length could only be statistically estimated using the average trace lengths from a surface and underground fracture mapping. Thus, fracture length is usually considered as the most uncertain parameter among the parameters related to hydraulic conductivity.

2. HYDROGEOLOGICAL CHARACTERIZATION OF THE STUDY AREA

2.1. Study Area

The study area was 3 km×5 km and located in the coastal region of the northern Yeosu peninsula in Jeonnam province, Korea. The rock types in this area consist mainly of volcanic rocks with granites intruded to its surroundings.

2.2. Surface Fracture Survey

In the study area, the fractures were surveyed at 30 selected outcrops using the scan line method. During the survey, fractures shorter than 1m were excluded. In the total survey length of 447 m, 935 fractures were detected. To classify the discontinuities observed in this study, the classification system used at SKB (Swedish Nuclear Fuel and Waste Management Company) was adapted (Black et al., 1994).

From the fracture data, four fracture sets were derived by using the FracMan (Golder Assoc. Inc., 1998) after Terzaghi (1965) correction. The fracture set 1, set 2 and set 3 is almost vertical fractures, while set 4 consists of low dip fractures. Figure 2 shows the projection of the fracture poles in stereographic net, indicating Fisher distribution. The fracture length was estimated from a forward modeling method (Dershowitz, 1995) based on the fracture trace lengths from the outcrop survey. The trace length of the four fracture sets in the study area shows mainly exponential distribution in Figure 3.

2.3. Borehole Fracture Survey

In order to investigate the subsurface fracture characteristics, a total length of 3290.03 m from 16 NX size boreholes was calculated using BHTV. Figure 4 is geology and location map of the study area. The borehole locations and azimuths were mainly based on geological structures assessed from the lineament analysis and enhanced by the surface geophysical investigation and surface fracture characteristics. For detailed fracture information around the boreholes, BHTV logging was carried out.

2.3.1. Fracture types

Since the purpose of this study was to predict groundwater flow, it was necessary to distinguish the conductive fractures on the assumption that groundwater can only flow

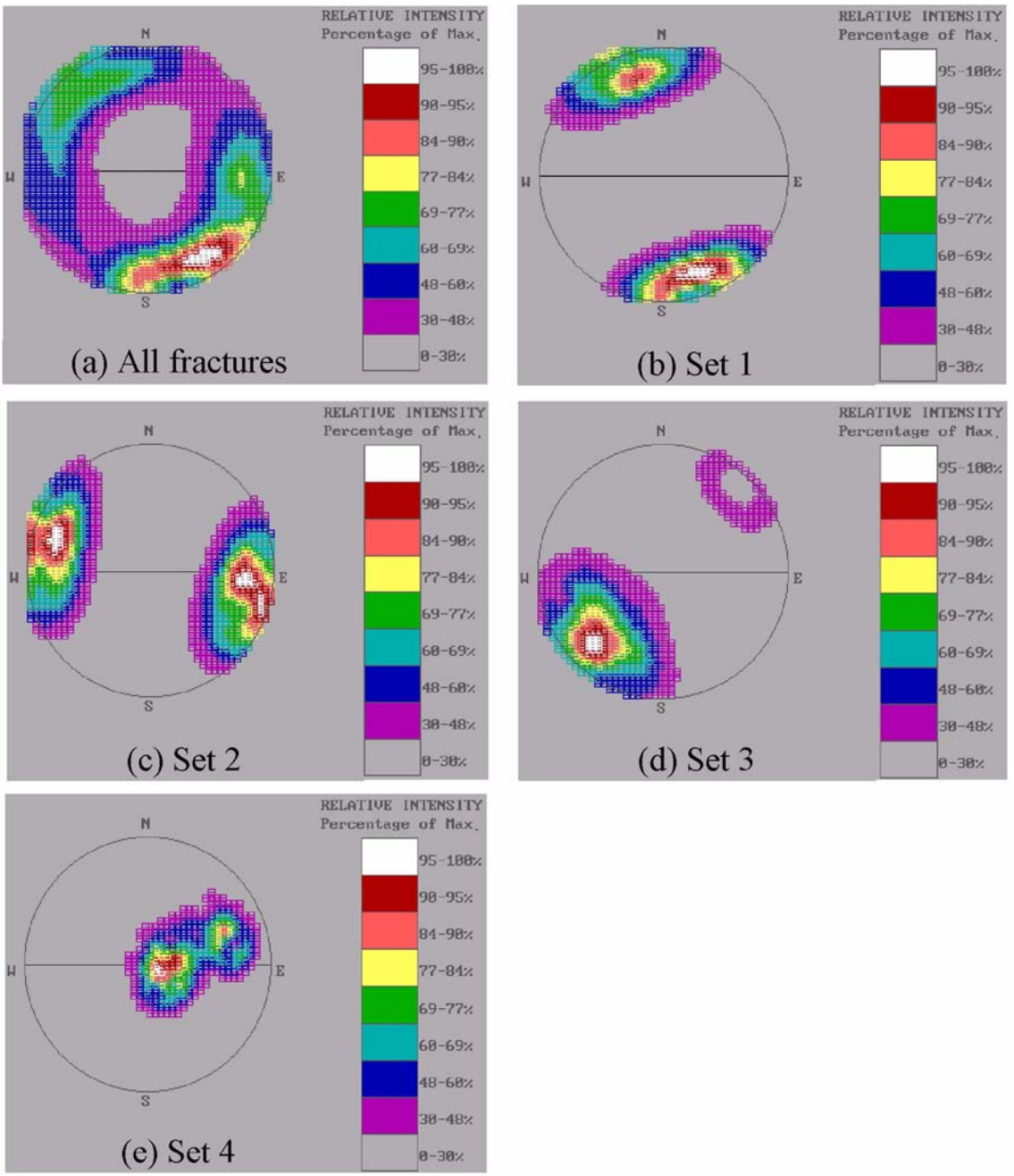

Fig. 2. Identification of the fracture sets from the surface fracture data.

through open fractures in a rock mass. The classification of a fracture was carried out on the basis of the level of detection on the amplitude and the travel time images of BHTV logging. When a fracture was detected on the amplitude image as well as on the travel time image, the fracture was regarded as an open fractures (Type 1). Fractures detected only on the amplitude image were regarded as closed fractures (Type 3).

As shown in Figure 5, the fracture frequencies depicted from the 16 boreholes are extremely high in the depth of GL (Ground Level) 0– –40 m. This can be considered as the weathered zone developed near surface. Therefore, the fracture network in this study was generated with Type 1 fractures after filtering out the fracture data from the surface to GL 40 m. After filtering out the near-surface fracture data, 694 open fractures were detected from 16 boreholes.

2.3.2. Fracture orientation

Figure 6 shows the stereographic projection for the fractures below GL –40 m. Figure 6b, c and d show three fracture sets determined from the FracMan Code. Fracture orientation was assumed to have a Fisher distribution (Priest,

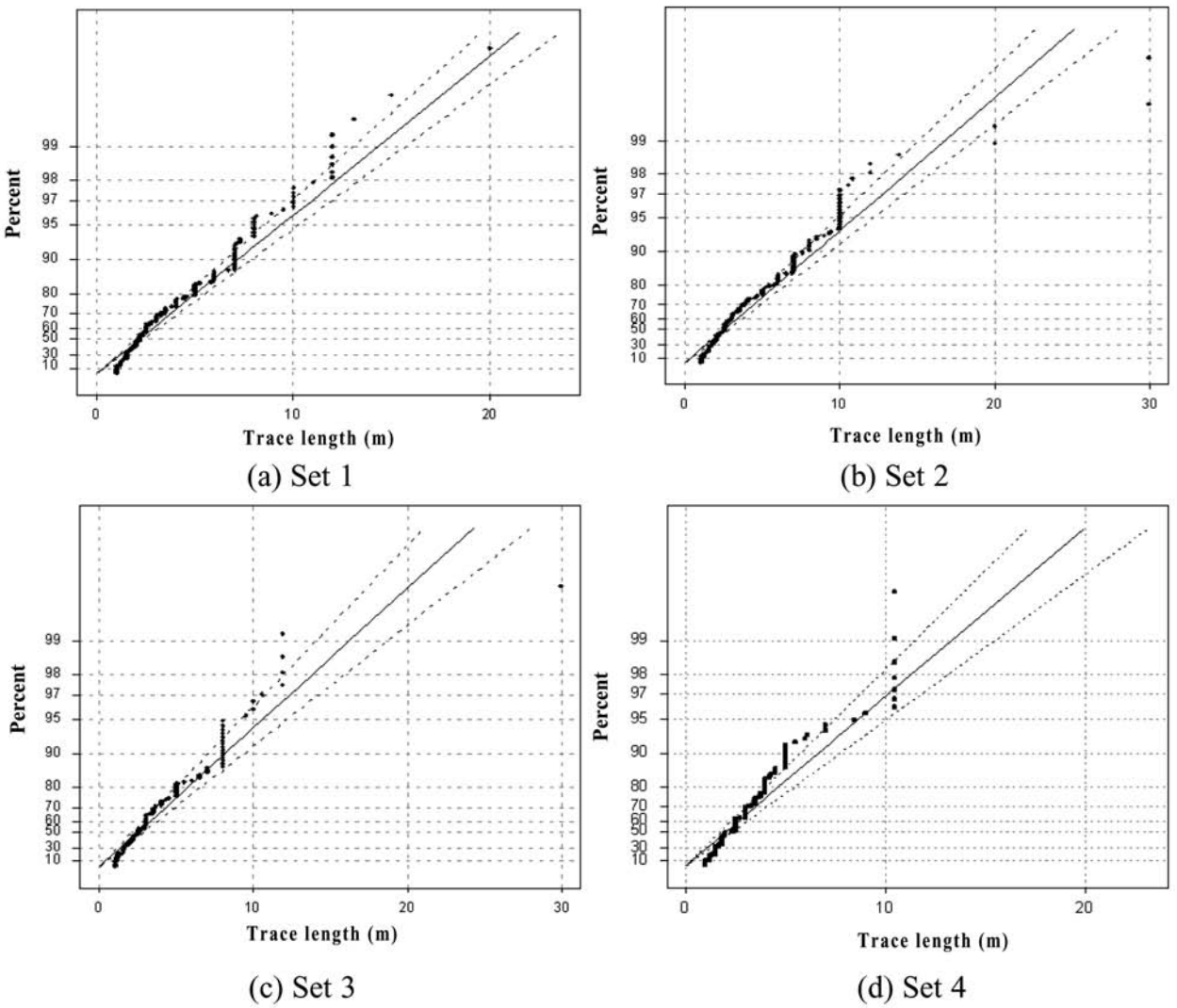

Fig. 3. Trace length distributions of the fracture sets.

1993). Table 1 lists the average values of dip, dip direction and Fisher Dispersion (K) of the fracture sets. The major dip directions are 155.2/87.6, 253.7/78.3 and 72.7/35.7. Fracture Sets 1 and 2 contain mostly vertical fractures, while Set 3 consists of sub-horizontal fractures with various dip directions.

2.3.3. Distribution of trace length

The trace length of each fracture set identified from the borehole survey can be obtained by comparing the distribution pattern of the fracture sets in stereographic net from the outcrop survey. Fracture Set 2 from the borehole is similar to fracture Set 3 of the outcrop survey, while fracture Set 3 is close to fracture Set 4 from the outcrop survey (refer to Figs. 2 and 6). The distribution pattern of the trace length of fracture Set 1 could be assumed as the same as that of fracture Set 1 of the outcrop survey. As shown in Figure 3, the distribution pattern of trace length of the fracture Set 1 is exponential and can be described using the following equation.

$$f(L) = C \cdot L^{-\lambda} \tag{1}$$

where L is trace length (m), C and λ are constants.

In this study, a truncated power-law distribution among the NAPSAC options was used. In that distribution model, the relationship between the trace length, L, and constant λ is

$$\text{mean } (L^2) = \frac{1-\lambda}{3-\lambda} \cdot \frac{L_{\max}^{3-\lambda} - L_{\min}^{3-\lambda}}{L_{\max}^{1-\lambda} - L_{\min}^{1-\lambda}} \tag{2}$$

where $L_{\max}$ and $L_{\min}$ are the maximum and minimum trace lengths (m), respectively. Constant C is

$$C = \frac{1-\lambda}{L_{\max}^{1-\lambda} - L_{\min}^{1-\lambda}} \tag{3}$$

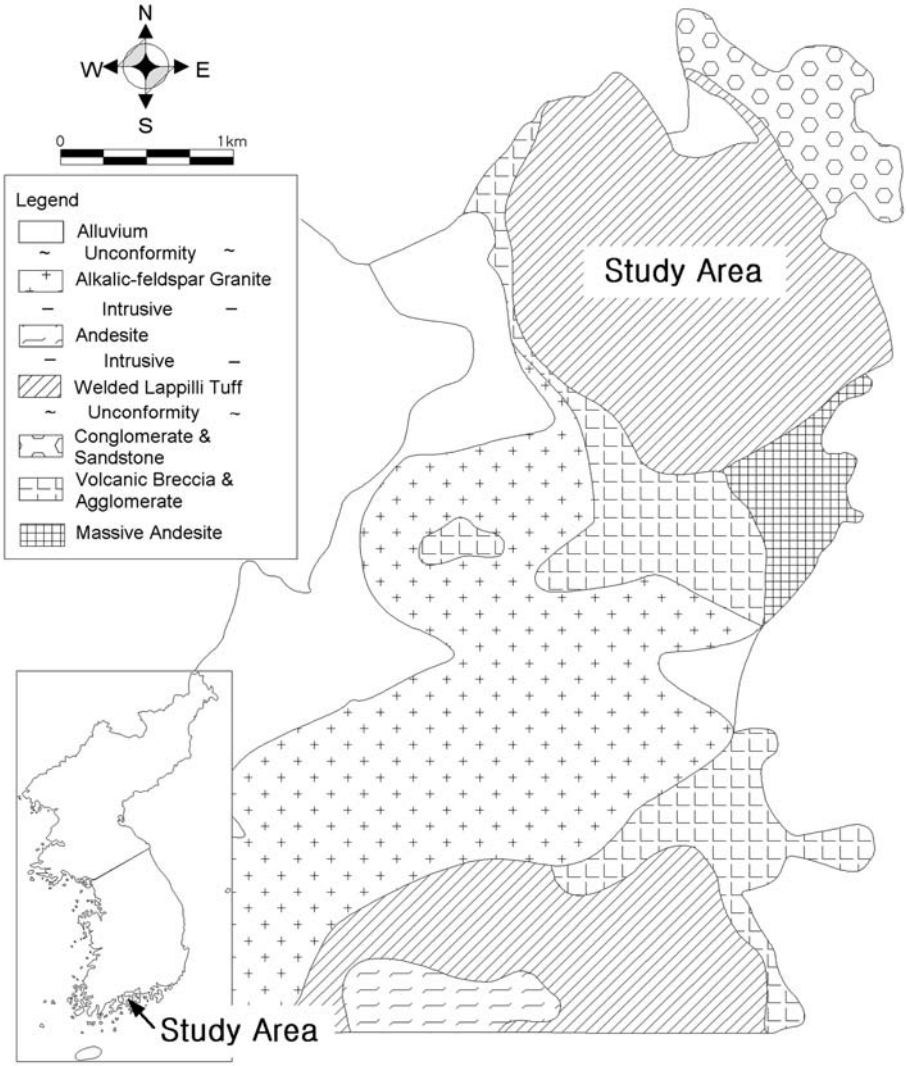

Fig. 4. Geology and location map of the study area.

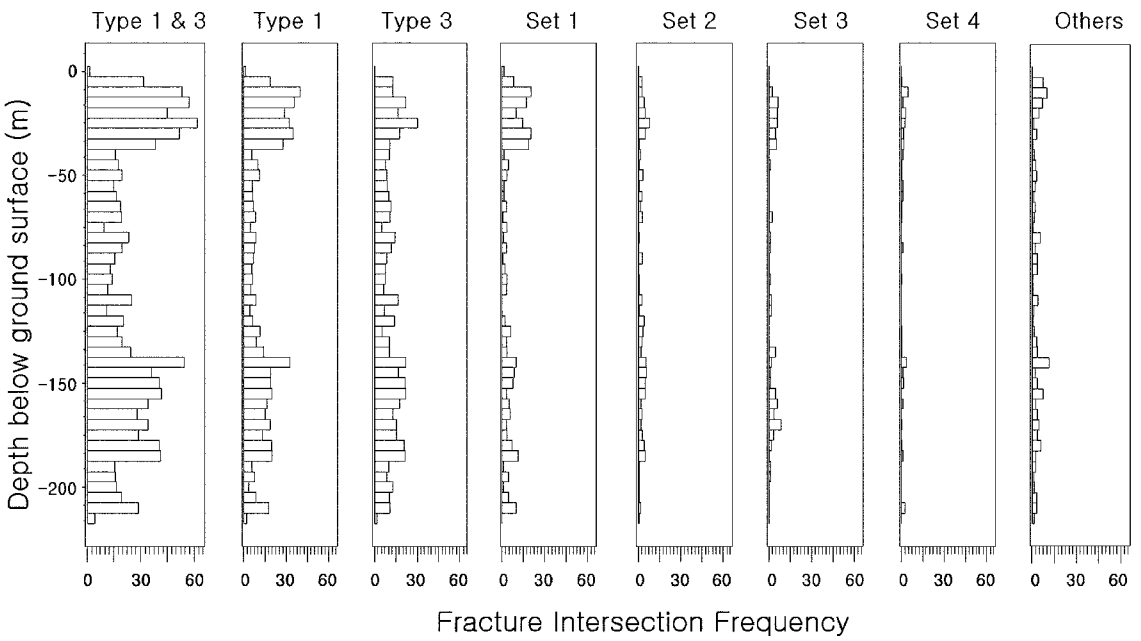

Fig. 5. Variation of the fracture frequencies in 16 boreholes along the depth.

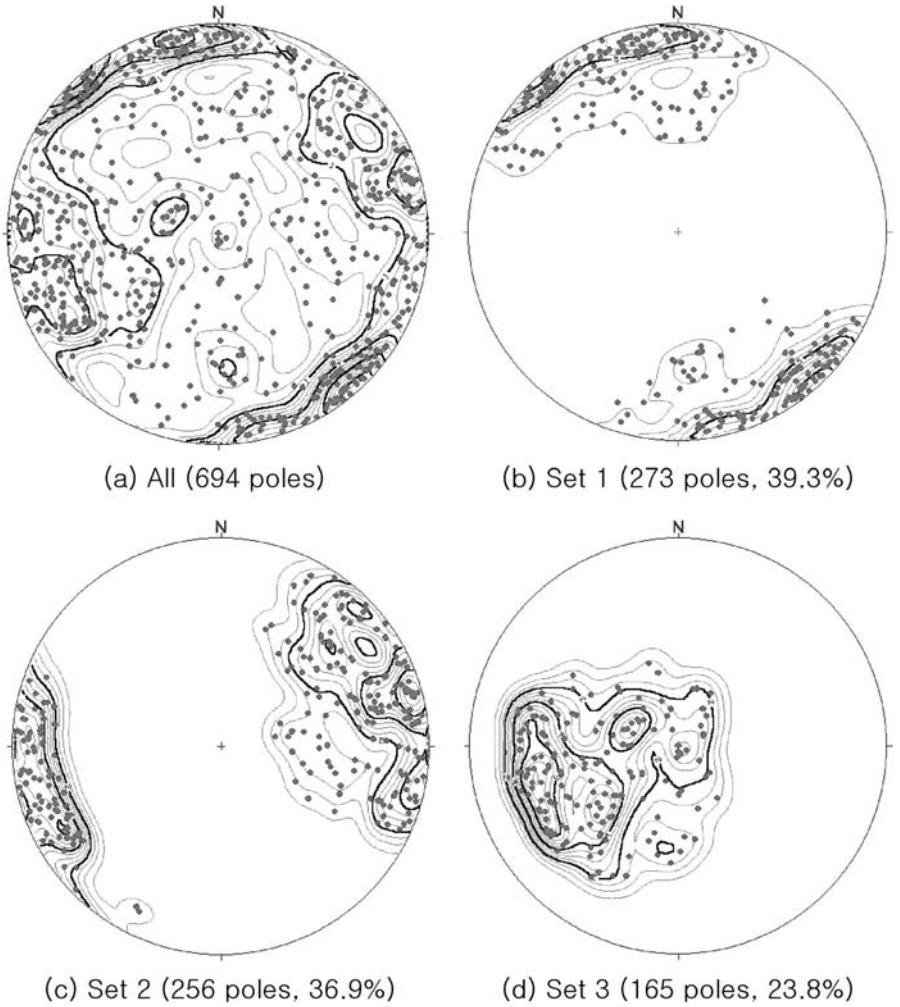

Fig. 6. Stereographic projection of the poles for the fractures below GL –40 m.

Table 1. Mean of the orientation and Fisher dispersion for each fracture set.

Item	Unit	Set 1	Set 2	Set 3
Mean (Dip Direction)	Degree	155.2	253.7	72.7
Mean (Dip Angle)	Degree	87.6	78.3	35.7
Fisher Dispersion (*K*)		8.4	7.4	7.7

Table 2. *C* and for each fracture set.

Item	Set 1	Set 2	Set 3
Mean (L^2)	16.497	22.970	13.005
L_{max}	20.0	30.0	10.5
L_{min}	1.0	1.0	1.0
λ	2.147	2.164	1.747
C	1.185	1.186	0.903

The constants C and λ are listed in Table 2. The required variables for generating the fracture network using NAPSAC are the maximum and minimum lengths and λ.

2.3.4. Fracture density

Fracture density is the key parameter for determining how many fractures will be included in a fracture network. An equivalent approach using a fracture density is to generate fractures in a specified area by the fracture density per unit volume. A Poisson process is used to generate the coordinates of the fracture centers. Care must be taken to avoid edge effect and that is usually accomplished by generating the fracture network in a larger region than that to be simulated. The fracture density can be determined from the spacing of fractures along a scan line on a mapped exposure, or from a fracture log along a borehole or core. For a given fracture set, the number density, ρ, is given in terms of the mean spacing of intersections along a straight line, $\bar{s}$ by (Hartley, 1998):

$$\bar{s} = (\lambda \bar{X})^{-1} \quad (4)$$

where $\bar{X}$ is the mean projected area of the fractures onto a plane perpendicular to the measurement line.

In order to determine this, it is necessary to consider the fracture length (L), fracture spacing (s), and dip (D) together. If those values are all random, the fracture density can be calculated from the average values as following:

Table 3. Fracture density of each fracture set.

Item	Unit	Set 1	Set 2	Set 3
Number of fractures		273 (39.3%)	256 (36.9%)	165 (23.8%)
Total vertical length of 16 boreholes	m	2787.06	2787.06	2787.06
Average fracture spacing (s)	m	10.21	10.89	16.89
Average fracture area (L^2)	m^2	16.497	22.970	13.005
Average cos (D)		0.222	0.0302	0.707
Fracture density	$/m^3$	0.027 (58.7%)	0.013 (28.3%)	0.006 (13.0%)

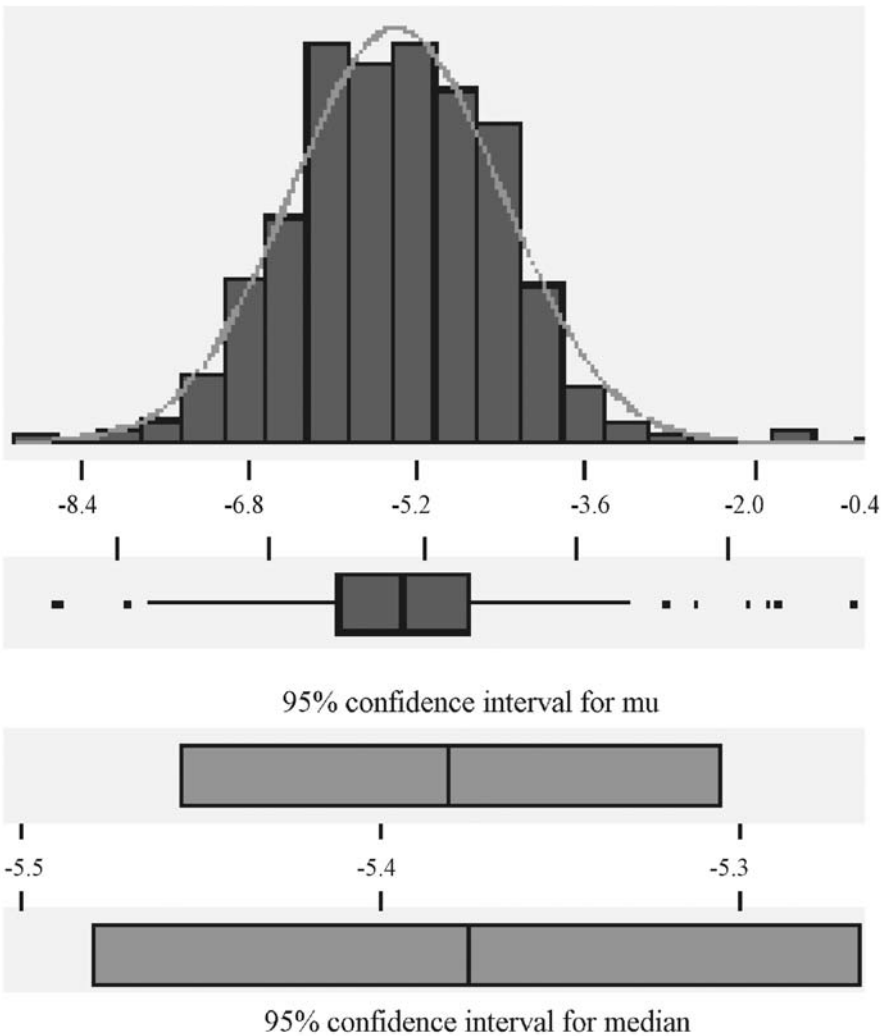

Fig. 7. Histogram for fracture aperture distribution.

$$\rho = \frac{1}{\text{mean}(s) \cdot \text{mean}(L^2) \cdot \text{mean}(\cos D)} \quad (5)$$

The estimated fracture densities of the study area, whose stereographic projection is in Figure 6, are listed in Table 3. The measuring distance of the 16 boreholes is 2787.06 m, which is obtained after extracting the upper 40 m of the boreholes from the total length of 3290.03 m.

Table 4. Statistics of the fracture aperture of the type 1 fractures below GL −40 m (unit: m).

	Set 1	Set 2	Set 3
Mean (aperture)	6.903E-3	9.221E-3	1.009E-2
STD (aperture)	1.224E-2	3.478E-2	1.934E-2
Mean (Ln(aperture))	-5.450	-5.462	-5.142
STD (Ln(aperture))	0.905	1.054	1.041

2.3.5. Fracture aperture

The aperture distribution of the open fractures of each fracture set below GL −40 m is shown in Figure 7. The three fracture sets can be fitted reliably by using straight lines,

and the aperture distribution is in a log-normal shape. Statistics of the fracture aperture of the Type 1 fractures are listed in Table 4.

2.4. Hydraulic Test

Two hundred and five constant pressure injection tests in eight boreholes and long-term pumping tests in two boreholes were carried out to evaluate the hydraulic properties of the area (Kim, 2000).

In the hydraulic tests, the injection pressure in a straddle packer was increased stepwise from 1 to 7 bars for 10 min. at each step. A packer interval of 9 m was used for the range from the surface to EL (Elevation Level) 0 m and a 6 m interval was used below EL 0 m.

Hydraulic conductivity can be calculated using the following equation suggested by Moye (1967).

$$K = \frac{q}{lH_0}\left[\frac{1}{2\pi}\left\{1 + \ln\left(\frac{1}{r_w}\right)\right\}\right] \quad (6)$$

where q is injection flow (m^3/s), l is interval of packers (m), H_0 is injection pressure (m), r_w is borehole diameter (m).

In order to minimize the calculation error, the average hydraulic conductivity after excluding the maximum and minimum values in each testing interval was calculated. Figure 8 shows the cumulative hydraulic conductivity of each borehole represented on a log-normal graph. The effective hydraulic conductivities from boreholes would be larger than the actual value because the data include the hydraulic conductivities from the upper regions with fractured and weathered zones. Thus, the depth down to GL −50 m was considered as an upper weathered zone and excluded for determining the in situ hydraulic conductivity of the rock mass in this study.

The effective hydraulic conductivity for rock mass was determined as 5.05×10^{-9} m/s based on the geometric means of the hydraulic conductivities of rock and fracture zones. With the same method, the effective hydraulic conductivity for the horizontal water curtain hole was determined as 8.56×10^{-9} m/s.

3. 3D DISCRETE FRACTURE NETWORK MEDELING

3.1. Geometry of Fracture Network

The fractures calculation in the NAPSAC model is too large for the study area of 6 km×5 km. Therefore, it was used for a three dimensional continuum model, which comprises the hydraulic characteristics of fractures on the study area scale. In order to reflect the hydraulic characteristics of fractures into a continuum model, the six components of hydraulic conductivity (K_{xx}, K_{yy}, K_{zz}, K_{xy}, K_{yz} and K_{zx}) should be determined to represent the site statistically. In addition, a cubic DFN model, which reflected the geometric and hydraulic fracture characteristics, was prepared to determine the above six components. Using the model, the anisotropic hydraulic conductivities of the block scale were determined and utilized to make a three-dimensional porous continuum model of the site using the NAMMU code. The continuum model is applicable for the groundwater flow analysis, if the directional hydraulic properties of the site are considered.

As mentioned earlier, dip/dip direction, fracture spacing and fracture length are the main parameters required to gen-

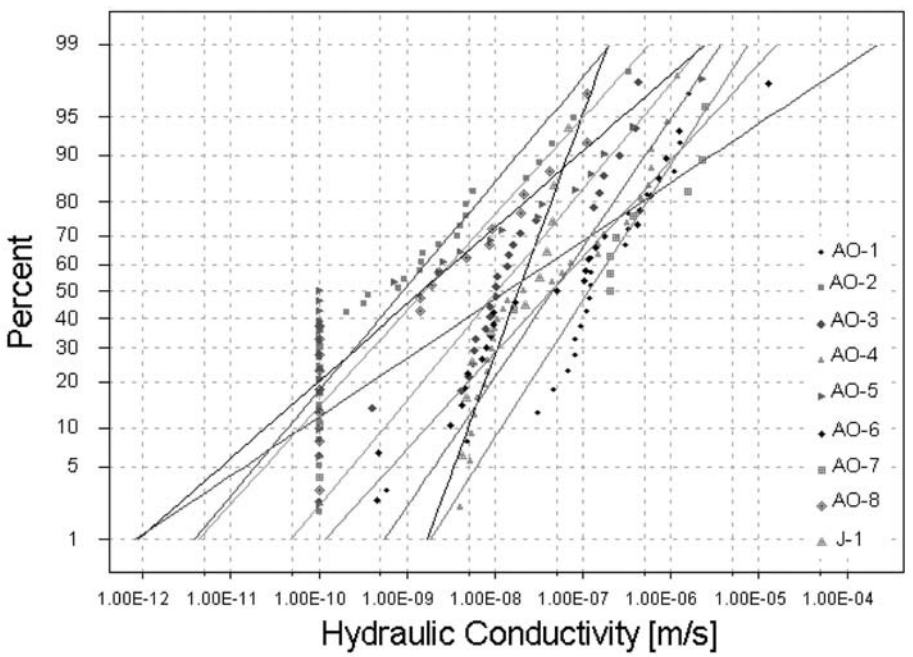

Fig. 8. Log-normal probability plot of the hydraulic conductivities in the boreholes.

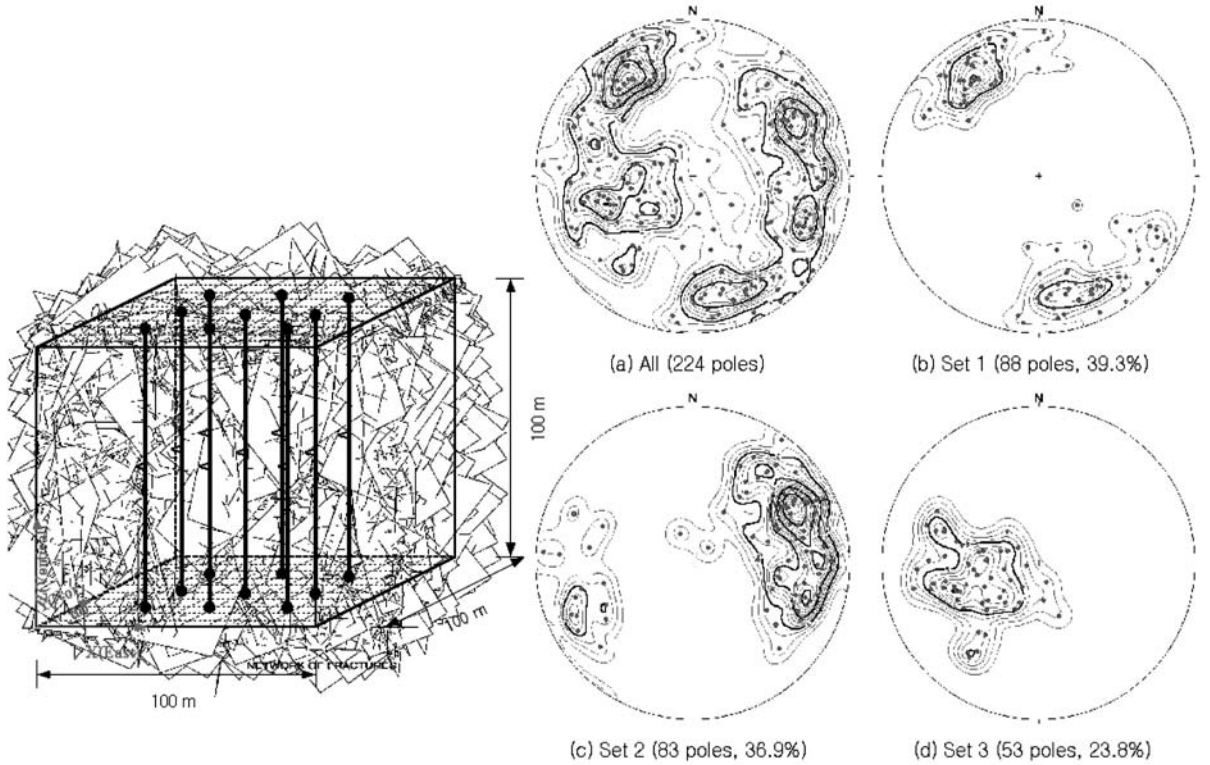

Fig. 9. Stereographic projection of the poles for the fractures of the fracture network generated from in-situ fracture data.

erate a fracture network. Fracture aperture is only related to the hydraulic conductivity and does not influence the fracture network geometry. Since dip/dip direction and fracture spacing were determined from the BHTV logging, they are the fundamental site-specific parameters. Therefore, fracture lengths can be considered as the only variable data for the deviation of the model results from the in situ measurements. Fracture length cannot be determined directly but needs to be estimated from the trace lengths obtained from the outcrop survey. Among the variables for exponential distribution in Table 2, the maximum and minimum values of fracture length derived from the surface survey cannot be changed. The parameter λ is the only one to be used to control the exponential distribution. Therefore, the fracture network was adjusted by changing λ. Because the constant C in Eq. 1 is a function of λ (Eq. 3), the distribution of each set can be controlled by adjusting λ.

The initial fracture network was generated in a cube with side length of 100 m using the NAPSAC model and the field data previously described. The fractures were generated by using the Monte Carlo method. For the random generation of the fractures, a seed number was already confirmed statistically (Park, 2000). Such an adjustment of λ for each fracture set by comparing the stereographic net in Figure 6 should be iterated until the final fracture network is established. Then, the final fracture network for the nine 100 m boreholes was plotted on a stereographic net as shown in Figure 9. The total 224 fractures from the nine 100 m boreholes were intersected and plotted on the net.

Because the ratios of poles of each set in the fracture distribution of the model are almost the same as those in Figure 6, the final fracture network can be regarded as statistically representative of the study area at the geometric point of view. The final λ for Sets 1, 2 and 3 are 2.240, 2.334 and 1.817, respectively. Those values were used to generate the fracture network and for deriving the hydraulic characteristics of the studied area.

3.2. Components of Hydraulic Conductivity

3.2.1. Hydraulic conductivity and transmissivity

The boundary condition is designed to determine the hydraulic conductivity of the study area. The fracture network was generated based on the parameters previously determined for each fracture set. It is possible to determine the six components of hydraulic conductivity as well as intrinsic permeability by imposing a certain hydraulic pressure of 400 Pa in the study area and maintaining 0 Pa at the point of interest in the model.

In NAPSAC, either hydraulic aperture or transmissivity can be specified to define the hydraulic response of fracture. The distribution of fracture apertures in this study displays a log-normal distribution (Section 2.3.4). It should be, however, kept in mind that the fracture apertures determined from BHTV are physical apertures and those should not be used as hydraulic apertures. Thus, the transmissivity

was used instead of the hydraulic aperture which could be calculated from a physical fracture aperture. The following equation was used for the transmissivity obtained from the in situ hydraulic conductivities measured.

$$K_e \cong \frac{T}{s} \tag{7}$$

where K_e, is effective hydraulic conductivity (m/s), T is a geometric mean transmissivity of individual fractures (m^2/s), and s is a spacing of open fractures (m).

To calculate the geometric mean of transmissivity from that of hydraulic conductivity, log space should be used. In log space, the geometric mean is the same as arithmetic mean. Thus, it is possible to determine the arithmetic mean using the following equation.

$$\ln(T) \cong \ln(K_e) + \ln(s) \tag{8}$$

This value was used as input data for the NAPSAC model and log-normal distribution was selected for the transmissivity distribution. Equation 7 was reported to be accurate when the fracture spacing and packer interval are similar (Hartley, 1998).

Table 5. Finally modified six components of hydraulic conductivity [unit: m/s].

Components	Boreholes	Horizontal water curtain holes
K_{xx}	4.3×10^{-9}	8.19×10^{-8}
K_{yy}	5.10×10^{-9}	7.82×10^{-8}
K_{zz}	6.32×10^{-9}	1.11×10^{-7}
K_{xy}	7.13×10^{-10}	1.17×10^{-8}
K_{yz}	-1.36×10^{-9}	-1.33×10^{-8}
K_{zx}	-4.44×10^{-10}	-3.05×10^{-10}
Geo. mean	5.05×10^{-9}	8.56×10^{-9}

Table 6. Six components of permeability corresponding to the hydraulic conductivities in Table 5 [unit : m^2].

Components	Boreholes	Horizontal water curtain holes
K_{xx}	4.48×10^{-16}	8.39×10^{-15}
K_{yy}	5.22×10^{-16}	8.01×10^{-15}
K_{zz}	6.47×10^{-16}	1.14×10^{-14}
K_{xy}	7.30×10^{-17}	1.20×10^{-15}
K_{yz}	-1.39×10^{-16}	-1.36×10^{-15}
K_{zx}	-4.55×10^{-17}	-3.12×10^{-17}
Geo. mean	5.17×10^{-16}	8.77×10^{-16}

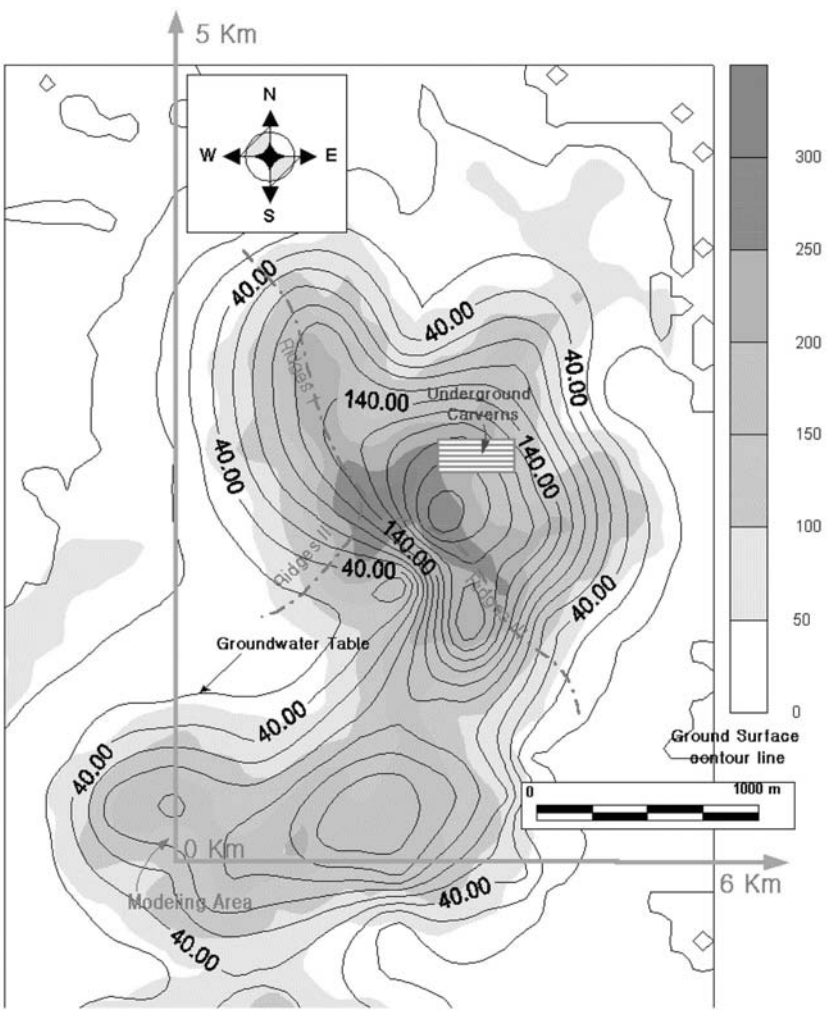

Fig. 10. Area for the modeling in the study area.

3.2.2. Anisotropic hydraulic conductivity and permeability

The packer intervals of the hydraulic test were in the range of six to nine meters. By considering the average fracture spacing of about one meter which is recommended from the NAPSAC model, six components of hydraulic conductivity were iterated to match the geometric hydraulic conductivities measured from boreholes and water curtain holes. Table 5 lists the final six anisotropic hydraulic conductivity components calculated from the fracture network by feedback calculation. Thus, it is possible to regard the six component of K as the in situ hydraulic characteristics of the rock mass.

By multiplying the conversion factor (ν/g), 1.0244×10^{-7} ($m \cdot s$), to the hydraulic conductivity, the intrinsic permeability of each component was determined and listed in Table 6. The permeability values can be used as input for the three-dimensional continuum model, NAMMU, to improve the calculation for the groundwater flow paths and travel times with consideration of in-situ condition.

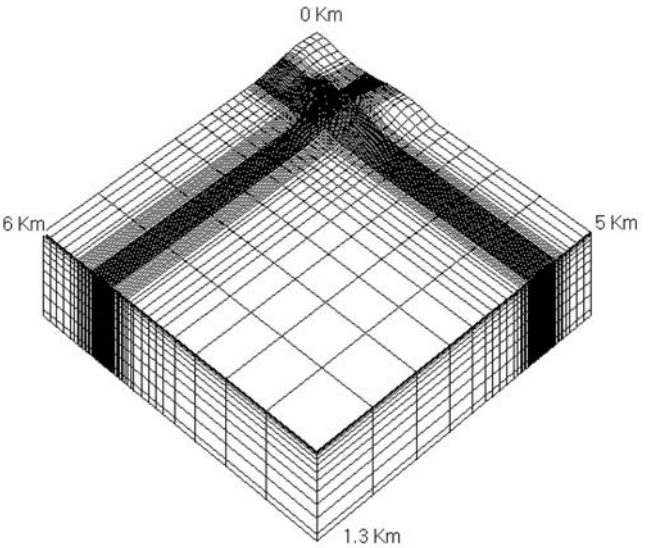

Fig. 11. Finite element model mesh in the study area.

4. GROUNDWATER SYSTEM ANALYSIS FOR THE UNDERGROUND CAVERNS EXCAVATION

The arrival times and the flow paths of groundwater from an underground cavern to the surface were determined with consideration of the complex mountainous topography in the study area, by using the anisotropic hydraulic conductivities previously calculated from the three-dimensional fracture network model.

4.1. Description of the Model

Figure 10 shows the modeling area and the location of the underground excavations. In order to solve the boundary condition problem, north and east boundary was extended to sea. Figure 11 shows the model mesh for NAMMU, inside of 6 km×5 km×1.3 km. The finite element mesh contains 49,590 nodes and 44,688 elements. Six caverns were included in the model. The width of the cavern was 20 m, the height was 30 m, the length was 400 m and the elevation of the cavern floor was selected to EL –60 m.

In order to confirm the reliability of the model, it was compared to the calculated groundwater inflow with the actual measurements from the nearby underground oil storage caverns constructed in the similar geological setting. The inflow rates into storage caverns estimated by continumm model ranged from about 130–140 m^3/day during the construction stage, whereas the inflow rates by actual measurements are 80–175 m^3/day.

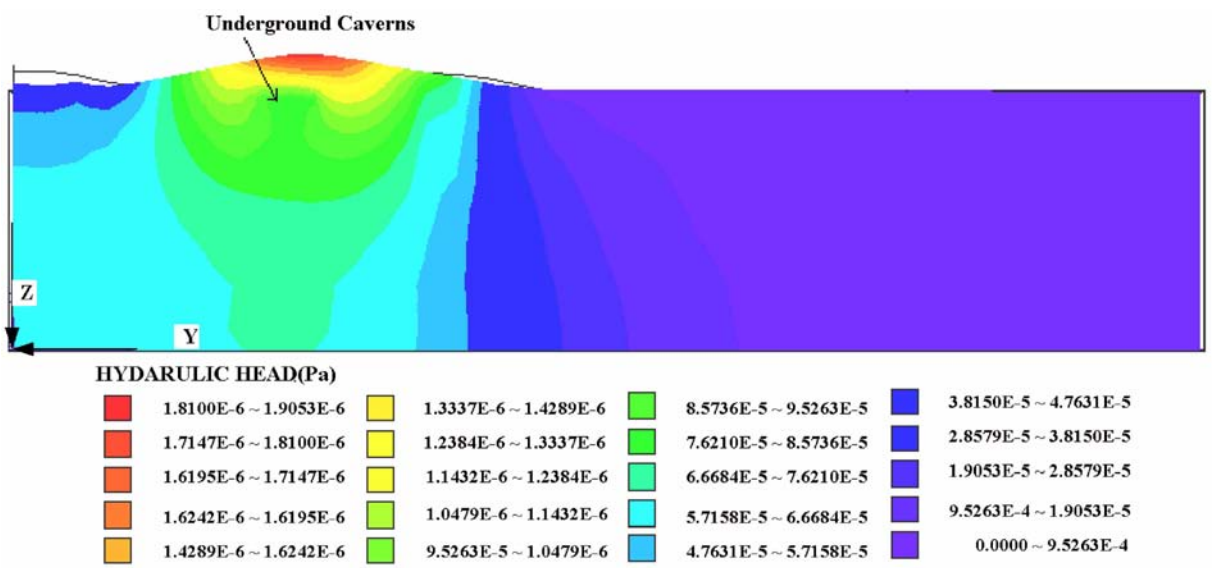

Fig. 12. Variation of hydraulic head after the underground caverns excavation (X direction view).

Table 7. Calculated groundwater inflow to the caverns (unit: m^3/day).

Caverns	Boreholes	Horizontal water curtain holes
Cavern 1	97.31	102.17
Cavern 2	103.63	108.81
Cavern 3	106.86	112.21
Cavern 4	107.69	113.07
Cavern 5	108.62	114.06
Cavern 6	113.47	119.14

4.2. Calculation Results

With minor adjustment, the numerical modeling is able to accurately reproduce groundwater inflows into the caverns. Figure 12 shows the changes of groundwater system after the underground excavation. Table 7 lists groundwater inflows into the caverns. Six different possible paths from different starting points to the surface were selected and the calculation of the travel times along each path was attempted. Two different models were used to evaluate the influence of anisotropic hydraulic conductivity. The first model uses the anisotropic hydraulic conductivities calculated from the surface based boreholes and the second uses the anisotropic hydraulic conductivities calculated from the horizontal water curtain holes in underground.

Figure 13 shows the eighteen flow paths from the caverns floor to the surface. Table 8 lists the travel lengths and the arriving times to the surface through the flow paths.

Table 8. Travel time to the surface through the flow paths for each cavern.

Path	Boreholes		Horizontal water curtain holes	
	Travel time (month)	Pathlength (m)	Travel time (month)	Pathlength (m)
1	27514	4542	29001	4788
2	4099	2184	4320	2302
3	148	880	156	928
4	34567	4749	36436	5006
5	6115	2501	6446	2636
6	175	933	185	983
7	39179	4922	41297	5188
8	9339	2838	9843	2991
9	729	1283	768	1352
10	44652	5032	47065	5304
11	11082	2979	11681	3140
12	1042	1354	1098	1428
13	47803	5044	50387	5317
14	12214	3055	12874	3220
15	2533	1655	2670	1744
16	46984	4974	49523	5243
17	11497	2992	12119	3154
18	2158	1530	2274	1613
Average	16768	2969	17675	3130

5. CONCLUSIONS

The anisotropic hydraulic conductivities determined from the in-situ hydraulic tests were applied to analyze the groundwater system. Anisotropic hydraulic conductivities are determined from a three-dimensional fracture network model, which is generated by using the fracture data from surface survey, borehole logging and hydraulic tests. The three-dimensional fracture network model could be matched geometrically with the in-situ conditions by compared to the stereographic nets of fracture data.

Total 694 data (Set 1 of 273, Set 2 of 256 and Set 3 of 165 data) of discontinuity were obtained from the statistical

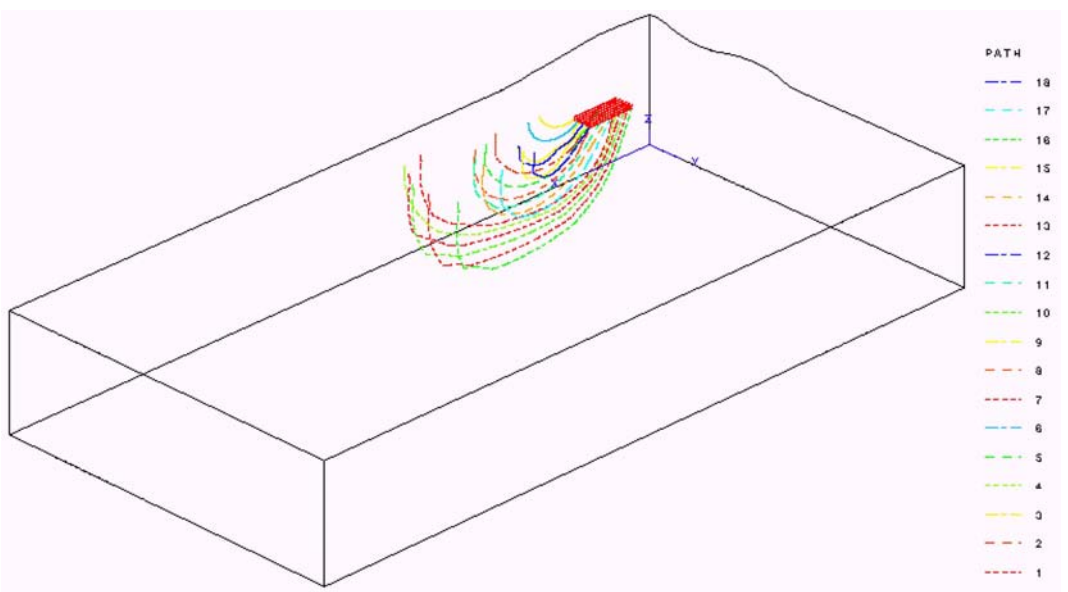

Fig. 13. The eighteen flow paths from the caverns floor to the surface.

analysis of permeable discontinuity in 16 boreholes. Total 224 data (Set 1 of 88, Set 2 of 83 and Set 3 of 53 data) of discontinuity were acquired from the 3D DFN modeling.

The anisotropic hydraulic conductivity values of six components, which are inversely calculated from a trial and error method using a 3D DFN model and the effective hydraulic conductivity (5.05×10^{-9} m/sec) of boreholes, are 4.37×10^{-9} m/sec, 5.10×10^{-9} m/sec, 6.32×10^{-9} m/sec, 7.13×10^{-10} m/sec, -1.36×10^{-9} m/sec and -4.44×10^{-10} m/sec, respectively.

The values of anisotropic hydraulic conductivity using a 3D DFN model and the effective hydraulic conductivity (8.56×10^{-9} m/sec) of horizontal water curtain hole data are 8.19×10^{-8} m/sec, 7.82×10^{-8} m/sec, 1.11×10^{-7} m/sec, 1.17×10^{-8} m/sec, -1.33×10^{-8} m/sec, -3.05×10^{-10} m/sec, respectively.

It is possible to calculate groundwater inflow to the caverns, pathways and travel times more realistically from the three-dimensional continuum model enhanced by the anisotropic hydraulic conductivities. It is very important to predict the pathway as well as the flow rate for potential oil leakage from underground oil storage caverns to protect facility and the environment.

In the case of complex mountainous topology, which is common in Korea, the travel times and pathways are strongly dependent on the location of leaking. It is, therefore, recommended to carry out three-dimensional modeling with consideration of hydraulic head variation depending on the terrain.

REFERENCES

Atkinson, R., Cherill, T.P., Herbert, A.W., Hodgkidon, D.P., Jackerson, C.P., Rae, J. and Robinson, P.C., 1984, Preview of the Groundwater Flow and Radionuclide Transport Modeling in KBS-3. UKAEA Report AERE-R, 11140, p. 84–125.

Bawden, W.F., 1980, Two-phase flow through rock fractures. Ph.D. thesis, Department of Civil Engineering, University of Toronto, p. 438–481.

Black, J.W., Dershowitz, W., Axelsson, K.L., Doe, T. and Been, K., 1994, Review of SKB framework for the geoscientific characterization of sites for deep repositories with emphasis on the testing and numerical representation of fractured crystalline rock. PR44-94-001, p. 126–148.

Dershowitz, W., 1995, Interpretation and synthesis of discrete fracuture orientation, size, shape, spatial structure and hydrologic data by forward modeling in fractured and jointed rock masses. In: Myer, L.R. and Tsang, C.F. (eds.), Proceedings of the Conference on Fractured and Jointed Rock Masses. Lake Tahoe, California, USA, June 3–5, A.A. Balkema, Rotterdam, p. 579–586.

Goodall, D.C., 1986, Containment of gas in rock caverns. Ph.D. thesis, Department of Civil Engineering, University of California, Berkley, p. 486–512.

Goodall, D.C., Aberg, B. and Brekke, T.L., 1988, Fundamental of gas containment in unlined rock caverns. Rock Mechanics and Rock Engineering, 21, 235–258.

Golder Association Incorporated, 1998, Fracman-Interactive discrete feature data analysis, geometric modeling, and exploration simulation (Version 2.603).

Geostock, 1992, LPG underground storage project in PyongtaekBasic design. Yukong Gas Ltd., p. 21–45.

Hartley, L.J., Brear, D.J., Cliffe, K.A. and Herbert, A.W., 1994, Integration of Discrete Representation of a Fracture Flow System with Continuum Approximations of Larger Scale Flow Away from the Region of Interest. DSAT(94)N24, p. 121–152.

Hartley, L.J., Cliffe, K.A., Herbert, A.W., Shepley, M.G. and Wilcock, P.M., 1995, Groundwater Flow Modeling with a Combined Discrete Fracture Network and Continuum Approach Using the Code 'NAMMU - NAPSAC'. DSAT Report DSAT(95)N8, p. 145–163.

Hartley, L.J., 1996, CONNECTFLOW (Release 1.0) User Guide. AEA Technology, Waste Environmental Group, AEAT-0527 (From http://www.connectflow.co.uk/).

Hartley, L.J., Herbert, A.W. and Wilcock, P.M., 1996, NAPSAC (Release 4.0) Summary Document. AEA Technology, AEA-D&R-027, p. 1–6.

Hartley, L.J., 1998, NAPSAC (Release 4.1) Technical Summary Document. AEA Technology, AEA-D&R-0271 (From http://www.napsac.co.uk/).

Hartley, L.J., Jackson, C.P. and Watson, S.P., 1996, NAMMU (Release 6.3) User Guide. AEA Technology, AEA-ES-0138 (From http://www.nammu.co.uk/).

Jenkins, K., Hock, A.R. and Wei, L., 1995, Transient Solver Crosscode Comparison between NAPSAC and FRACMAN/MAFIC. Golder Associates Inc., p. 276–312.

Kim, K.S., 2000, Hydrogeological Stability Study on the Underground Oil Storage Caverns by Numerical Modeling. Ph.D. thesis, Chungnam National University, Daejeon, Korea, p. 99–111.

Moye, D.G., 1967, Diamond Drilling for Foundation Exploration. Civil Engineering Transactions, Institution of Engineers, Australia, CE9, p. 95–100.

Nakagawa, K., Komada, H., Miyashita, K. and Murata, M., 1987, Study on compressed air storage in unlined rock caverns. 6th International ISRM Congress on Rock Mechanics, Montreal, Canada, p. 86–93.

Park, B.Y., 2000, Three dimensional Numerical Model Analysis of the Change of Groundwater System with Cavern Excavation in Volcanic Rocks. Ph.D. thesis, Seoul National University, Seoul, Korea, p. 81–102.

Priest, S.D., 1st ed., 1993, Discontinuity Analysis for Rock Engineering. Chapman & Hall, p. 87–92.

Robison, P.C., Jackerson, C.P., Herbert, A.W. and Atkinson, R., 1986, Review of the Groundwater Modeling of the Swiss Project Gewähr. UKAEA Report AERE-R, 11929, p. 139–156.

Schwartz, F.W. and Lee, G., 1991, Cross-verification Testing of Fracture Flow and Mass Transport Codes. Stripa Project Techical Report 91-29, SKB, Stockholm, p. 64–85.

Terzaghi, R., 1965, Source of Error in Joint Surveys. Geotechnique, 15, 287–304.

Watanabe, K., Ishiyama, K. and Asaeda, T., 1987, Instability of the interface between gas and liguid in an open fractured model. 6th International ISRM Congress on Rock Mechanics, Montreal, Canada, p. 94–102.

Manuscript received April 29, 2004
Manuscript accepted December 6, 2004